ADVANCED OPTICAL MATERIALS
www.advopticalmat.de

Matching Photocurrents of Sub-cells in Double-Junction Organic Solar Cells via Coupling Between Surface Plasmon Polaritons and Microcavity Modes

Yu Jin, Jing Feng, Ming Xu, Xu-Lin Zhang, Lei Wang, Qi-Dai Chen, Hai-Yu Wang, and Hong-Bo Sun**

Organic photovoltaics offer a potentially low-cost, flexible, lightweight, and large-area source of renewable energy.[1] Recently, much work on designing new materials,[2] device structures[3] and processing techniques[4] has been carried out to improve the power conversion efficiency (PCE) of organic solar cells. So far, efficiencies of ~8% for small molecule[5] and ~10% for polymer devices[6] have been acheived. However, further improvements are still required for their commercial application. In particular, the open-circuit voltage (V_{oc}) needs to be improved for their ideal application in driving low-power electronic devices, typically to ~4.2 V.[7] Tandem configurations, in which two or more single cells are stacked in series, have been accepted as a successful and universal strategy to increase the V_{oc} of the devices.[8] A record of up to 7 V for six-junction solar cells has been reported.[9] However, the photocurrent of the tandem cells is usually lower than that of the single-junction cells, because less light is absorbed by the back sub-cell compared to the front one in a typical tandem device, which creates an imbalance in the photocurrent generated by the back and front sub-cells, and limits the PCE of the overall device. Therefore, matching the photocurrent of the back and front sub-cells is crucial for a high PCE of the tandem organic solar cell.

Appropriate choice of materials with different bandgaps can overcome this problem to a certain degree.[10] However, this approach is difficult to apply to multi-junction organic solar cells, especially for small molecule-based cells, due to the limited choice of the small-molecule donor materials that have significantly different absorption profiles. Careful design of the optical field and photovoltaic contributions from the sub-cells is another strategy to optimize the tandem cell. Surface plasmon polariton (SPP)-induced field enhancement has been believed to be a highly attractive solution to enhance optical obsorption in an organic solar cell without increasing the thickness of its active layers.[11] SPPs are described as confined light waves propagating along the interface between a metal and a dielectric or semiconductor material.[12] SPPs can be excited in solar cells by employing a metallic nanostructure, such as metallic nanoparticles,[13] and a periodically nanopatterned metal film.[14] In this Communication, SPP resonance has been employed in the small molecule-based double-junction organic solar cells with two identical sub-cells to enhance the optical absorption of the back sub-cell by employing periodical corrugation in the metallic cathode. Both the SPP and microcavity modes are supported by the corrugated device structure, and the SPP resonance is tuned by tuning the period of the corrugation, so that an anti-crossing between the SPP and microcavity modes within the device is realized. This anti-crossing plays an important role in enhancing the absorption of the back sub-cell, and thereafter achieving a balanced photocurrent of front and back sub-cells, which results in an improved PCE for the double-junction device. Both simulation and experimental results support the effect of the anti-crossing behavior on the absorption enhancement. 10.4% enhancement in the photocurrent, and 11.3% enhancement in the PCE have been achieved in the double-junction devices with this periodical corrugation.

Boron subphthalocyanine chloride (SubPc) was used as the donor material (**Figure 1**(a)), and fullerene (C_{60}) was used as the acceptor material in both sub-cells in this work. Figure 1(b) schematically illustrates the structure of the corrugated double-junction devices, where the corrugation was introduced into the device by holographic lithography. The fabrication process of the corrugation is shown in Figure S1.[15] The 1D corrugations with various periods from 250 to 400 nm were fabricated on the surface of photoresist film. The surface profile of the corrugation with 300 nm grating period is shown in **Figure 2**(a), and the groove depth was determined to be around 80 nm (inset in Figure 2(a)). The following electrode and organic layers were deposited by thermal evaporation. Ag nanoparticle (Ag NP)/MoO_3 was used as the interlayer. The Au and Ca/Ag were used as anode and cathode, respectively, which formed a metal-mirror microcavity structure in the solar cells. To clarify the sequential structures of the front and back sub-cells after the depositon process, the cross section of the corrugated device was investigated by scanning electron microscopy (SEM) measurement. Figure 2(b) shows the image of the corrugated device at 90°. The front and back sub-cells both display corrugated structures, and the interlayer of Ag NP/MoO_3 is visible. The top surface of the corrugated and planar devices were also scanned by SEM and are shown in Figure 2(c) and (d); they exhibit identical morphology to that of the substrate. The SEM results indicate that the profile of the deposited layers is essentially a

Y. Jin, Prof. J. Feng, M. Xu, X.-L. Zhang, L. Wang, Prof. Q.-D. Chen, Prof. H.-Y. Wang, Prof. H.-B. Sun
State Key Laboratory on Integrated Optoelectronics
College of Electronic Science and Engineering
Jilin University
2699 Qianjin Street, Changchun, 130012, PR China
E-mail: jingfeng@jlu.edu.cn; hbsun@jlu.edu.cn
Prof. H.-B. Sun
College of Physics
Jilin University
119 Jiefang Road, Changchun, 130023, PR China

DOI: 10.1002/adom.201300223

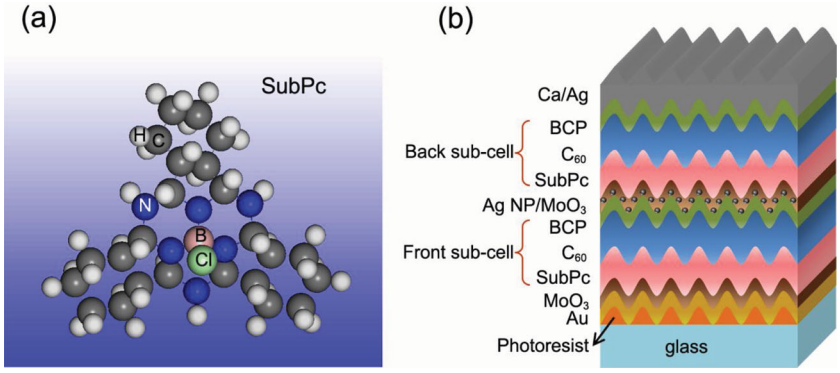

Figure 1. (a) Chemical structure of the donor material boron subphthalocyanine chloride. (b) Schematic structure of the corrugated double-junction solar cells.

replication of the underlying substrate, forming a periodic corrugation throughout the structure.

Understanding of the SPP effect on the absorption starts from analyzing the absorption spectra of the tandem devices. **Figure 3** shows the measured absorption spectra of planar and corrugated double-junction devices with various periods, which were obtained from the complementary relation between reflection and absorption. For the planar device, two absorption peaks appear at around 510 nm and 620 nm. For the corrugated device with the period of 400 nm, an additional peak appears at around 700 nm, which blueshifts with decreasing period and becomes undistinguishable due to its overlap with the absorption peak at 620 nm. When the period decreases to 300 and 250 nm, a broadband absorption enhancement is observed at around 600 nm compared to that of the planar tandem solar cells, which coincides with the intrinsic absorption of SubPc.

The optical modes in the planar and corrugated devices were identified by simulating both the absorption spectra and the spatial magnetic field (H_y) intensity distribution across the device structure by employing the finite-difference time-domain (FDTD) method.[16] A corrugation with sinusoidal cross section and fill factor of 50% was employed in the simulation. The refractive index of the organic materials employed in the solar cells was measured by ellipsometry and is shown in Figure S2. The simulated absorption spectra of the planar and corrugated devices with various periods are shown in Figure S3, which exhibit agreement with the experimental measurements. **Figure 4**(a) and (b) show the simulated field distribution for the planar device at wavelengths of 510 and 650 nm, respectively. It can be seen that the high field intensity at the two wavelength positions are both confined within the device, which is assigned to the standing-wave microcavity modes due to the light reflection between the two metallic electrodes. The optical resonance condition for light in the microcavity can be described as[17]

$$\sum_i n_i d_i + \frac{\lambda}{4\pi}(\varphi_1 + \varphi_2) = \frac{m\lambda}{2} \quad (1)$$

where n_i and d_i are refractive index and thickness of the layers between two mirrors, respectively, φ_1 and φ_2 are the phase change upon reflection from two mirrors, and m is a positive integer. There are two wavelengths satisfying the equation simultaneously, due to the anomalous dispersion of the SubPc at the wavelength region from 500 to 600 nm, as shown in Figure S2, where the refractive index promptly increases with the increase of wavelength. Therefore, the two absorption peaks at 510 nm and 620 nm both originate from microcavity resonance in the planar double-junction organic photovoltaic (OPV) as shown in Figure 3, which almost cover the intrinsic absorption region of SubPc from 500 to 620 nm.

Figure 4(c) shows the field distribution of the corrugated device with a 300-nm period at the wavelength of 650 nm. It can be seen that the field intensity exhibits its maximum mainly at the Ag cathode/back sub-cell interface and decays exponentially into both media, and in particular, extends to the SubPc layer of the back sub-cell. Combined with the blueshift of this mode with decreasing period, it can be assigned to the SPP resonance at the Ag cathode/back sub-cell interface. Meanwhile, the microcavity mode also exists at this interface. Figure 4(d) shows the dispersion map for the corrugated devices, in which the absorption intensity appears as a function of both grating periods and absorption

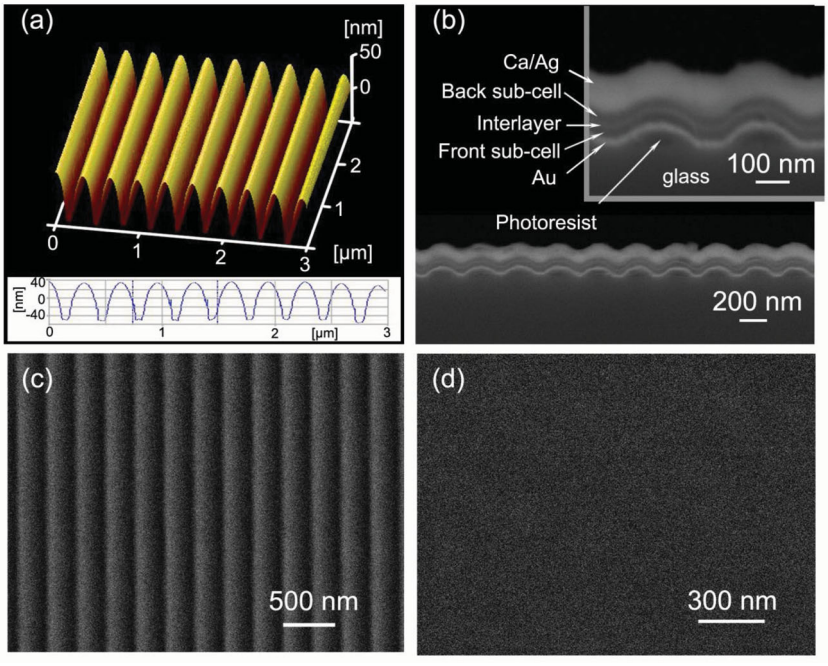

Figure 2. (a) Atomic force microscopy (AFM) image of the 1D corrugation on the photoresist surface, and the inset is the cross section. (b) SEM cross section of the corrugated device. (c,d) Top-view SEM images of the corrugated and planar double-junction solar cells, respectively.

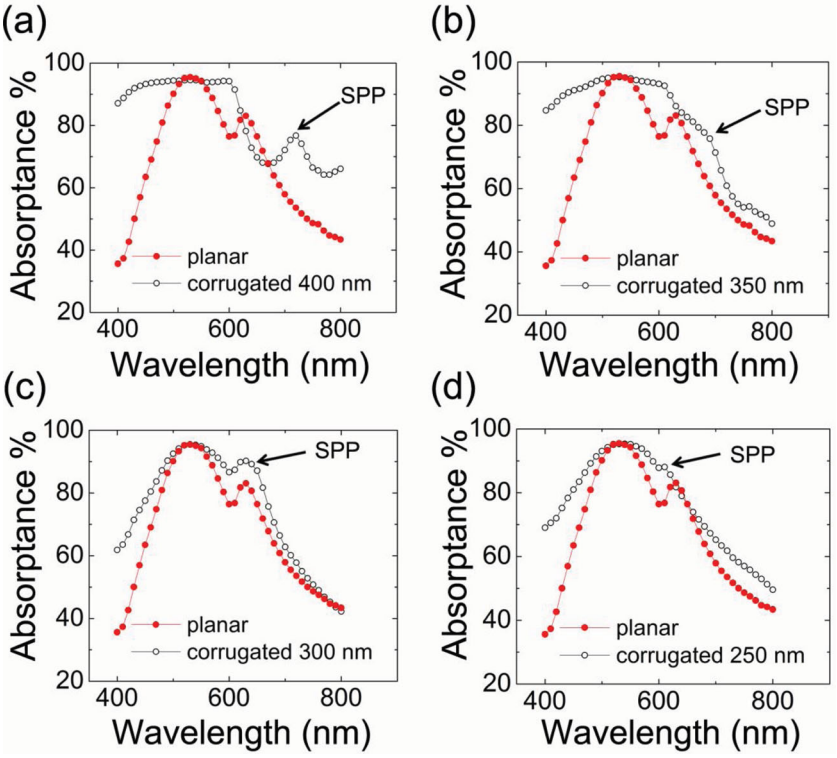

Figure 3. The experimentally measured absorption spectra of the planar and corrugated double-junction solar cells with periods of 400 nm (a), 350 nm (b), 300 nm (c) and 250 nm (d).

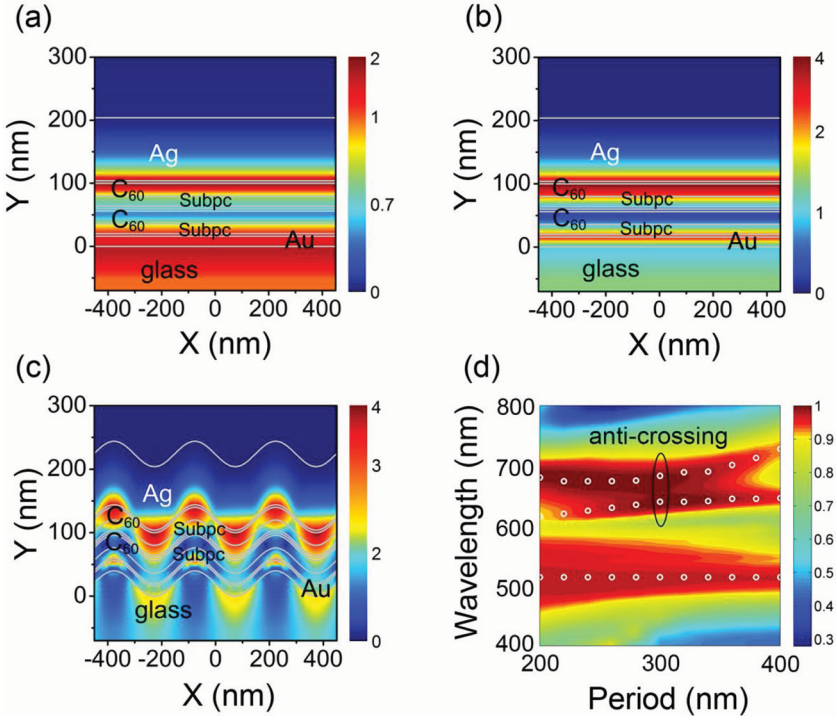

Figure 4. Distribution of the magnetic field intensity in the planar double-junction cells at the wavelengths of 510 nm (a), 650 nm (b), and the corrugated double-junction cells with period of 300 nm at the wavelength of 650 nm (c). (d) Dispersion relationship for the wavelength versus the period of the corrugation of the corrugated double-junction cells.

wavelengths. It can be seen that the peak of the SPP resonance exhibits a blueshift with decreasing period, and an anti-crossing between the SPP mode and microcavity mode occurs when the period is decreased to around 300 nm. This anti-crossing is caused by strong interference between the SPP and microcavity modes at the Ag cathode/back sub-cell interface. Anti-crossing between the SPP and microcavity modes has been reported in the metal–dielectric–metal structure, in which a strong field enhancement could be obtained.[18] Moreover, it leads to a broadband resonance at around 600 nm due to the formation of a large anti-crossing gap. We can conclude from the theoretical results that the improved absorption for the corrugated cells originates from the field enhancement induced by the anti-crossing between the SPP and microcavity modes, and the enhancement is mainly from the back sub-cell. It would improve the balance of the photocurrent between the back and front sub-cells. Notably, the absorption ranging from 400 nm to 500 nm also exhibits significant enhancement as shown in Figure 3, which corresponds to the absorption of C_{60}, and can be attributed to the elongated optical path of the incident light by scattering from the corrugated electrodes.[19] Therefore, a broadband absorption enhancement in the back sub-cell is obtained for the corrugated solar cells.

To verify the effect of the field enhancement induced by the anti-crossing on the photocurrent, current density–voltage (J–V) curves of the solar cells with different structures were measured and are shown in **Figure 5**(a). Device A and device B are single-junction and double-junction planar solar cells, respectively. Device C is a corrugated double-junction solar cell with a period of 300 nm. The V_{oc} of the planar and corrugated double-junction devices is the same, and is nearly twice the V_{oc} of the single-junction devices, as expected.[20] It suggests that the Ag NPs/MoO_3 interlayer does not introduce any electrical losses and the introduction of corrugation does not increase the interface resistance. In case of the short-circuit current density (J_{sc}), the planar double-junction solar cells exhibit lower J_{sc} compared to that of the planar single-junction solar cells, which is caused by the imbalance of absorption between the back and front sub-cells. However, the J_{sc} of the double-junction solar cells with the periodic corrugation is improved and even higher than that of the single-junction solar cells. The improved

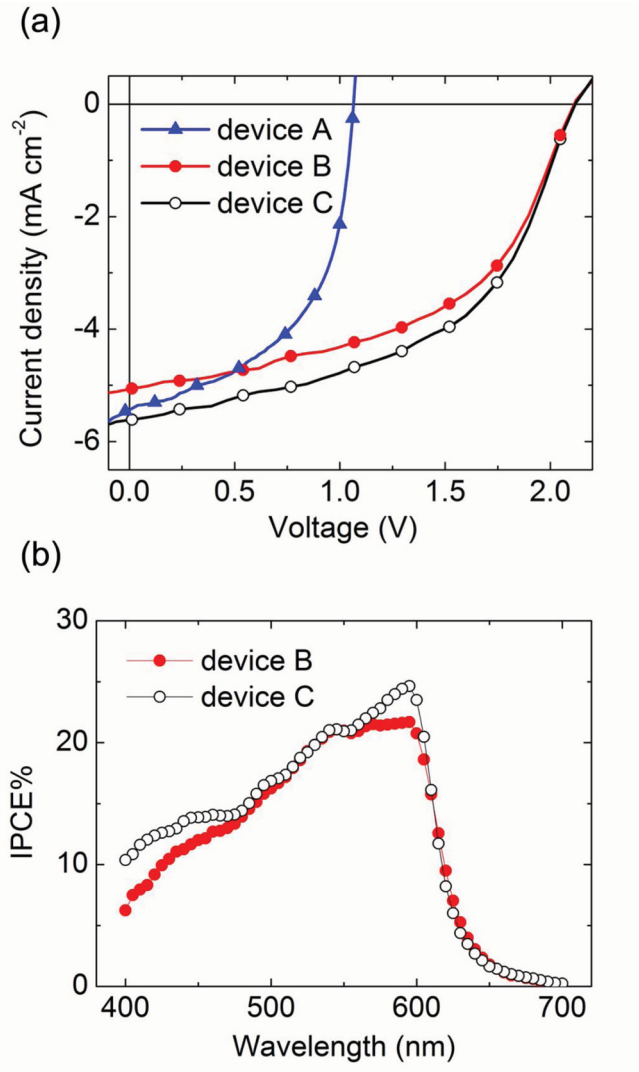

Figure 5. (a) J–V characteristics of the devices A, B, and C. (b) IPCE spectra of the planar (device B) and corrugated (device C) double-junction solar cells.

balance of the photocurrent in both back and front sub-cells induced by the anti-crossing contributes to this improvement, and the improved absorption of C_{60} due to the elongated optical path induced by the corrugation may also contributes to the improved J_{sc}. The detailed results are given in **Table 1**. The J_{sc} of the corrugated double-junction solar cells (device C) is 5.63 mA cm^{-2}, which corresponds to an enhancement of 10.4%

Table 1. The photovoltaic parameters of the planar single-junction cell (device A), the planar double-junction cell (device B), and the corrugated double-junction cell (device C).

	J_{sc} [mA cm^{-2}]	V_{oc} [V]	FF [%]	PCE [%]
Device A	5.43	1.1	51	3.07
Device B	5.10	2.1	51	5.48
Device C	5.63	2.1	51	6.10

compared to that of the planar double-junction OPV (device B, 5.10 mA cm^{-2}). As a result, the PCE of the corrugated device (device C) is increased to 6.1%, which shows an 11.3% enhancement compared to that of the planar device (device B, 5.48%).

The absorption enhancement due to the anti-crossing-induced field enhancement is further verified by comparing the measured incident photon to current conversation efficiency (IPCE) spectra of the corrugated and planar double-junction solar cells, as shown in Figure 5(b). The IPCE spectra shows obvious enhancement in the absorption region of SubPc for the corrugated device C compared to that of the planar device B, which is identical with their absorption spectra, as shown in Figure 3(c), and attributes to anti-crossing-induced field enhancement. Meanwhile, the enhancement of IPCE from 400 nm to 500 nm is attributed to the elongated optical path of the incident light scattering by the corrugated electrodes.

In conclusion, the optical absorption of the back sub-cell in the double-junction organic solar cells has been enhanced by strong coupling between the microcavity and propagating SPP modes at the Ag/back sub-cell interface by employing a periodic wavelength-scale corrugation into the device structure. The SPP resonance has been tuned to the intrinsic absorption wavelength of the photovoltaic material through tuning the period of the corrugation, and coincides with that of the microcavity mode, which results in their anti-crossing and leads to the field enhancement at the absorption region of the SubPc. Therefore, the optical absorption of the back sub-cell is improved and matched to that of the front sub-cell. As a result, the photocurrent is improved by 10.4% and a PCE of 6.1% is achieved, which is an 11.3% enhancement.

Experimental Section

Preparation of Periodically Corrugated Substrate: The process steps for fabrication of periodical corrugation by holographic lithography are shown in Figure S1. A continuous laser with 266 nm wavelength (Coherent Inc.) was used as irradiance light source. A 120-nm-thick layer of photoresist (NOA-68, Norland Inc.) was spin-coated onto the cleaned glass substrate and exposed to two beams which were split from the laser with beam size of ~6 mm in diameter. The spatial period is defined by the angle between the two laser beams. After exposure, the sample was baked for 1 min at 95 °C and then developed in acetone. The morphologies of the microstructure were characterized by atomic force microscopy (AFM, Digital Instruments Nanoscope IIIA) in tapping mode.

Solar Cell Fabrication and Evaluation: The corrugated and planar cells were both fabricated on glass substrates with or without the corrugated photoresist. The substrates were loaded into a thermal evaporation chamber. A 15-nm-thick Au layer (~10 Ω/square) was deposited onto the substrates by thermal evaporation through a shadow mask as the anode. 5-nm MoO_3 anodic modification layer, front sub-cell, Ag nanoparticles (Ag NPs 0.3 nm)/MoO_3 (5 nm) interlayer, back sub-cell and Ca (3 nm)/Ag (100 nm) cathode were evaporated sequentially. The front and back sub-cells were both using 18-nm boron subphthalocyanine chloride (SubPc) as the donor, 25-nm fullerene (C_{60}) as the acceptor, and 4-nm bathocuproine (BCP) as an exciton block layer. Organic and metallic films were thermally evaporated under high vacuum (5×10^{-4} Pa). All organic materials were purchased from LumTec. Corp. and used as received. The active area of the device is 2 mm × 2 mm. The thickness of each layer was monitored by quartz crystals and calibrated by a spectroscopic ellipsometer (J. A. Woollam Co., Inc. USA). Over 50 separate devices with and without corrugation were fabricated. The current density–voltage (J–V) curves of all solar cells were measured

by a Keithley 2400 sourcemeter under 1 sun simulated AM 1.5 G illumination (100 mW cm^{-2}). The results given in the paper are the average values. The reflectance spectra of the samples were measured by a UV–vis spectrophotometer (UV-2550, SHIMADZU Co., Inc. Japan). The cross section and the surface morphologies of the solar cells were characterized by a field emission scanning electron microscope (SEM, JSM-7500F, JEOL, Japan).

Supporting Information

Supporting Information is available from the Wiley Online Library or from the author.

Acknowledgements

The authors gratefully acknowledge support from the 973 Project (2011CB013005) and NSFC (Grant Nos. 91233123, 61177024, and 61107024).

Received: May 26, 2013
Revised: July 4, 2013
Published online: August 13, 2013

[1] a) J. Y. Kim, K. Lee, N. E. Coates, D. Moses, T. Q. Nguyen, M. Dante, A. J. Heeger, *Science* **2007**, *317*, 222; b) A. Nattestad, A. J. Mozer, M. K. R. Fischer, Y. B. Cheng, A. Mishra, P. Bäuerle, U. Bach, *Nat. Mater.* **2010**, *9*, 31; c) A. Hadipour, B. D. Boer, P. W. M. Blom, *Adv. Funct. Mater.* **2008**, *18*, 169.

[2] Z. Tang, Z. George, Z. Ma, J. Bergquist, K. Tvingstedt, K. Vandewal, E. Wang, L. M. Andersson, M. R. Andersson, F. L. Zhang, O. Inganäs, *Adv. Energy Mater.* **2012**, *2*, 1467.

[3] a) S. Kim, J. H. Koh, J. H. Kim, E. Kim, *J. Nanosci. Nanotechnol.* **2013**, *13*, 2632; b) S. E. Park, S. Kim, K. Kim, H. E. Joe, B. Jung, E. Kim, W. Kim, B. K. Min, J. Hwang, *Nanoscale* **2012**, *4*, 7773; c) J. Kim, J. K. Koh, B. Kim, H. Kim, E. Kim, *Angew. Chem. Int. Ed.* **2012**, *51*, 6864; d) D. H. Wang, J. Seifter, J. H. Park, D. G. Choi, A. J. Heeger, *Adv. Energy Mater.* **2012**, *2*, 1319; e) E. D. Kosten, J. H. Atwater, J. Parsons, A. Polman, H. A. Atwater, *Light: Sci. Appl.* **2013**, *2*, e45.

[4] a) S. Fabiano, Z. Chen, S. Vahedi, A. Facchetti, B. Pignataro, M. A. Loi, *J. Mater. Chem.* **2011**, *21*, 5891; b) A. Hadipour, B. D. Boer, J. Wildeman, F. B. Kooistra, J. C. Hummelen, M. G. R. Turbiez, M. M. Wienk, R. A. J. Janssen, P. W. Blom, *Adv. Funct. Mater.* **2006**, *16*, 1897.

[5] J. Meiss, T. Menke, K. Leo, C. Uhrich, W. M. Gnehr, S. Sonntag, M. Preiffer, M. Riede, *Appl. Phys. Lett.* **2011**, *99*, 043301.

[6] a) H. Y. Chen, J. H. Hou, S. Q. Zhang, Y. Y. Liang, G. W. Yang, Y. Yang, L. P. Yu, G. Li, *Nature Photon.* **2009**, *3*, 649; b) Y. Y. Liang, J. B. Xia, S. T. Tsai, Y. Wu, G. Li, C. Ray, L. P. Yu, *Adv. Mater.* **2010**, *22*, E135; c) F. Robert, *Science* **2011**, *332*, 293.

[7] B. Sahu, G. A. Rincón-Mora, *IEEE Tans. Power Electron.* **2004**, *19*, 443.

[8] a) D. Cheyns, B. P. Rand, P. Heremans, *Appl. Phys. Lett.* **2010**, *97*, 033301; b) M. Riede, C. Uhrich, J. Widmer, R. Timmreck, D. Wynands, G. Schwartz, W. M. Gnehr, D. Hildebrandt, A. Weiss, J. Hwang, S. Sundarraj, P. Erk, M. Pfeiffer, K. Leo, *Adv. Funct. Mater.* **2011**, *21*, 3019.

[9] P. Sullivan, S. Schumann, R. D. Campo, T. Howells, A. Duraud, M. Shipman, R. A. Hatton, T. S. Jones, *Adv. Energy Mater.* **2013**, *3*, 239.

[10] a) J. Gilot, M. M. Wienk, R. A. J. Janssen, *Adv. Mater.* **2010**, *22*, E67; b) L. Dou, J. B. You, J. Yang, C. C. Chen, Y. J. He, S. Murase, T. Moriarty, G. Li, Y. Yang, *Nature Phton.* **2012**, *6*, 180.

[11] a) Y. Jin, J. Feng, X. L. Zhang, M. Xu, Y. G. Bi, Q. D. Chen, H. Y. Wang, H. B. Sun, *Appl. Phys. Lett.* **2012**, *101*, 163303; b) T. Shimada, S. Tomita, S. Hotta, S. Hayashi, H. Yanagi, *Jap. J. Appl. Phys.* **2009**, *48*, 042001; c) H. A. Atwater, A. Polman, *Nature Mater.* **2010**, *9*, 205213; d) C. Cocoyer, L. Rocha, L. Sicot, B. Geffroy, R. D. Bettignies, C. Sentein, C. Fiorini-Debuisschert, P. Raimond, *Appl. Phys. Lett.* **2006**, *88*, 133108; e) J. K. Mapel, M. Singh, M. A. Baldo, K. Celebi, *Appl. Phys. Lett.* **2007**, *90*, 121102; f) D. Duche, P. Torchio, L. Escoubas, F. Monestier, J. J. Simon, F. Flory, G. Mathian, *Sol. Energy Mater. Sol. Cells* **2009**, *93*, 1377; g) B. P. Devi, K. C. Wu, Z. Pei, *Sol. Energy Mater. Sol. Cells* **2011**, *95*, 2102.

[12] W. L. Barnes, A. Dereux, T. W. Ebbesen, *Nature* **2003**, *424*, 824.

[13] a) K. Imura, H. Okamoto, Y. Nishijima, K. Ueno, H. Misawa, *J. Appl. Phys.* **2011**, *110*, 104306; b) Y. Yokota, K. Ueno, V. Mizeiki, S. Juodkazis, K. Sasaki, H. Misawa, *J. Nanophoton.* **2007**, *1*, 011594; c) K. Ueno, H. Misawa, *Phys. Chem. Chem. Phys.* **2013**, *15*, 4093; d) W. J. Toon, K. Y. Jung, T. Duraisamy, R. Revur, F. L. Teixeira, S. Sengupta, P. R. Berger, *Sol. Energy Mater. Sol. Cells* **2010**, *94*, 128; e) A. J. Morfa, K. L. Rowlen, T. H. Reilly III, M. J. Romero, J. V. D. Lagemaat, *Appl. Phys. Lett.* **2008**, *92*, 013504; f) S. S. Kim, S. I. Na, J. Jo, D. Y. Kim, Y. C. Nah, *Appl. Phys. Lett.* **2008**, *93*, 073307; g) A. P. Kulkarni, K. M. Noone, K. Munechika, S. R. Guyer, D. S. Ginger, *Nano. Lett.* **2010**, *10*, 1501.

[14] a) K. Tvingstedt, N. K. Persson, O. Inganäs, A. Rahachou, L. V. Zozoulenko, *Appl. Phys. Lett.* **2007**, *91*, 113514; b) M. A. Sefunc, A. K. Okyay, H. V. Demir, *Appl. Phys. Lett.* **2011**, *98*, 093117; c) A. Abass, H. H. Shen, P. Bienstman, *J. Appl. Phys.* **2011**, *109*, 023111; d) M. Niggemann, M. Glatthaar, A. Hinsch, V. Wittwer, *Thin Solid Film* **2004**, *451*, 619; e) C. J. Min, J. Li, G. Veronis, J. Y. Lee, S. Fan, P. Peumans, *Appl. Phys. Lett.* **2010**, *96*, 133302; f) A. Williamson, É. McClean, D. Leipold, D. Zerulla, *Appl. Phys. Lett.* **2011**, *99*, 093307.

[15] Y. Jin, J. Feng, X. L. Zhang, Y. G. Bi, Y. Bai, L. Chen, T. Lan, Y. F. Liu, Q. D. Chen, H. B. Sun, *Adv. Mater.* **2012**, *24*, 1187.

[16] X. L. Zhang, J. Feng, J. F. Song, X. B. Li, H. B. Sun, *Opt. Lett.* **2011**, *36*, 3915.

[17] Y. B. Long, *Appl. Phys. Lett.* **2009**, *95*, 193301.

[18] a) Z. Chen, I. R. Hooper, J. R. Sambles, *J. Opt. Soc. Am. A* **2007**, *24*, 1084; b) L. Fu, P. Schau, K. Frenner, W. Osten, T. Weiss, H. Schweizer, H. Giessen, *Phys. Rev. B* **2011**, *84*, 235402; c) R. Ameling, H. Giessen, *Nano Lett.* **2010**, *10*, 4394.

[19] Y. Jin, J. Feng, Y. H. Wang, M. Xu, T. Lan, Y. G. Bi, Q. D. Chen, H. Y. Wang, H. B. Sun, *IEEE Photo. J.* **2012**, *4*, 1737.

[20] D. Cheyns, B. P. Rand, P. Heremans, *Appl. Phys. Lett.* **2010**, *97*, 033301.